Influence of Fluorine implantation on the physical and electrical characteristics of GaN-on-GaN vertical Schottky diode.

Vishwajeet Maurya, Julien Buckley, Daniel Alquier, Helge Haas, Mohamed-Reda Irekti, Thomas Kaltsounis, Matthew Charles, Névine Rochat, Camille Sonneville, Veronique Sousa

Influence of Fluorine implantation on the physical and electrical characteristics of GaN-on-GaN vertical Schottky diode

Vishwajeet Maurya [a,b], Julien Buckley [a], Daniel Alquier [b], Helge Haas [a], Mohamed-Reda Irekti [a], Thomas Kaltsounis [a], Matthew Charles [a], Névine Rochat [a], Camille Sonneville [c], Veronique Sousa [a]

[a] Univ . Grenoble Alpes, CEA, Leti , F 38000 Grenoble, France

[b] GREMAN UMR 7347, Université de Tours, CNRS, INSA Centre Val de Loire, 37071 Tours, France

[c] Univ. Lyon, INSA Lyon, Univ. Claude Bernard Lyon 1, Ecole Centrale Lyon, CNRS, Ampère, 69621, Villeurbanne, France

Abstract

Fluorine implantation has been reported to be effective in suppressing electric fields at the edge of Schottky contacts in GaN due to the formation of fixed negative charged traps. In this study we show a detailed investigation into the behavior of fluorine implantation in GaN on material and electrical properties, and reproduce these electrical properties using TCAD simulations. A reduction in the free carrier concentration is observed by both µ-Raman, SSRM and C-V measurements, likely due to the trapping of free electrons by fluorine ions. The barrier height extracted from C-V measurements increases with increasing implant overlap area under the Schottky contact, whereas the barrier height extracted from I-V measurements remains constant. For the device without any implantation, the extracted barrier height remained the same for both extraction methods. This observation suggests the existence of a high and low double barriers originating from the implant and non-implant region respectively. TCAD simulations performed by including negative charge support the formation of a double barrier. By using the barrier height extracted from C-V measurements for the implanted region, we were able to use our TCAD model to estimate the profile of fixed negative charge, which is around 10 % of the total implanted fluorine. This understanding shows that for effective design of edge terminations using fluorine implantation, consideration of the fixed negative charge as a percentage of the fluorine implantation is very important.

Keywords

Vertical GaN, Schottky, fluorine implantation, Synopsys TCAD, edge termination

1. Introduction

GaN-based power devices have been gaining popularity in recent years thanks to GaN properties such as wide bandgap, high electron mobility and high breakdown field strength, allowing low R_{on} and high-frequency operation for high voltage devices. Lateral GaN devices, which are typically grown on a foreign substrate such as silicon [1] , have already been commercialized and have been able to achieve much better performance compared to their silicon counterparts. However, with these devices, achieving high breakdown voltages (>1kV) is highly challenging. The recent availability of high quality native GaN substrates gives the opportunity to fabricate vertical devices, which boost both breakdown voltage and lower R_{on} even further. However, these devices still suffer from premature breakdown and high reverse leakage due to electric field crowding at the junction edge. Among the various existing solutions in literature, this issue can be resolved by creating an effective edge termination either by using magnesium implantation [2] to create a p-doped junction barrier region or by alternate species implantation such as nitrogen [3] or argon [4] to create a resistive region at the junction edge due to the damage related defects [5]. However, due to the difficulty in creating p-type GaN areas by Mg implantation, which requires cap-layers associated with complicated rapid thermal annealing (RTA) [6] or very high pressure and temperature annealing to activate the dopants [2], alternate species are preferred. Fluorine ion implantation is an attractive alternative as it can form a negative fixed charge, owning to its high electronegativity, and so spread the electric field away from the contact and modulate the free charge carrier in GaN. Fluorine implantation in GaN is not a new research topic. It has been investigated for GaN HEMT devices based on AlGaN/GaN hetrostructures, where it was used to deplete the high-density 2-dimensional electron gas (2-DEG) to obtain normally off devices [7]. In recent years, several research groups have been able to enhance the breakdown voltage of vertical GaN Schottky devices using fluorine [8][9], validating the effectiveness of fluorine implantation in spreading the electric field away from the Metal-Semiconductor (M-S) contact edge. However, limited literature is available on the underlying physics. In this work, to investigate and get a better insight into the impact of fluorine implantation, we have studied the Schottky barrier or built-in potential by varying the implanted area under the Schottky contact using current-voltage (I-V) or capacitance-voltage (C-V) techniques, respectively. In addition, various physical characterizations have been used to characterize the ion-implanted region and provide information on the doping variations.

2. Experiment

2.1. Epitaxial growth and Schottky diode fabrication

The GaN epitaxial layers were grown on a 2" diameter substrate from Saint Gobain Lumilog with n-type doping and thickness of 2×10^{18} cm^{-3} and 300 µm respectively. The epitaxial layer was grown by using metal-organic vapor phase epitaxy (MOVPE) in a closed coupled showerhead reactor. A 10 µm thick n^- GaN layer with silicon doping was grown on the Gallium face of the substrate with a net doping concentration of around 1.3×10^{16} cm^{-3}.

The fabrication of the Schottky diodes started with the deposition of a Ti/Al/Ni/Au metal stack on the backside of the wafer followed by an RTA annealing at 850°C to form the Ohmic contact. Then, a SiO_2 hard mask was deposited by PECVD on the top side of the wafer, which was selectively etched to open the surface for fluorine implantation. Multi-energy implantation using 30, 60, and 100 keV was carried out with ion fluence of 6×10^{13} cm^{-2}, 3×10^{13} cm^{-2} and 1×10^{13} cm^{-2} respectively. The sample was tilted by 7° relative to the incident beam to prevent implanted ion from channeling into the GaN. Post implantation, an RTA at 400°C was carried out in an N_2 atmosphere for 10 minutes to reduce implant damage related defects. Circular Ni/Au Schottky contacts were patterned using lift-off and the contact was annealed at 350°C under N_2 environment. The fabricated devices were passivated using Al_2O_3/SiN/SiO_2 layers. The passivation was then opened to make contacts for the electrical measurements. A schematic cross-section of the fabricated structure is shown in Fig. 1(a). A non-implanted structure was also fabricated for reference.

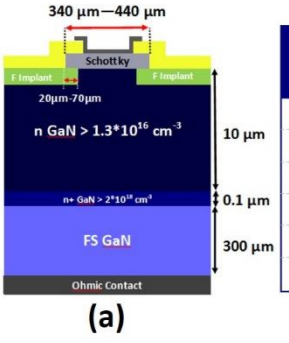

Device	Anode Radius (µm)	Non Implant Radius (µm)	Implant Overlap Length (µm)	Implant Area/ Total Area
Device 1	170	150	20	0.22
Device 2	180	150	30	0.31
Device 3	190	150	40	0.38
Device 4	200	150	50	0.44
Device 5	210	150	60	0.5
Device 6	220	150	70	0.54

(b)

Figure 1. (a) Schottky device structure.(b) 6 devices (named as Device 1 to Device 6) with a constant non-implant inner area and increasing implant overlap under the Schottky contact were fabricated along with a non-implanted diode.

2.2. Characterization methodology

To characterize the impact of fluorine implant on the GaN epitaxial layer, both physical and electrical characterizations were performed after the implantation process. Scanning spreading resistance microscopy (SSRM)

and Atomic Force Microscopy (AFM) were conducted using a Burker Dimension ICON tool to evaluate the surface properties. SSRM measurement is AFM based electrical mode with the capability of mapping two-dimensional resistivity in a semiconductor. µ-Raman mapping using a Renishaw inVIA^{TW} confocal Raman microscope in backscattering geometry and with a laser excitation at 532 nm was used to investigate the impact on the doping as the A_1(LO) peak position of the Raman spectra is sensitive to local variation in the doping density. Cathodoluminisence (CL) mapping was also performed to examine the impact on the luminescence properties of the implanted area. For electrical characterization, I-V measurements were performed at room temperature (RT) using a Keithley 1500A source measure unit (SMU) and breakdown measurements were conducted using a Keithley 2657A high-power SMU. To extract the doping density and barrier height, C-V measurements were conducted using an HP4510 impedance analyzer.

3. Results and discussions

3.1. Implanted GaN region

Fig. 2(a)-(b) shows the AFM image acquired from the implanted and non-implanted GaN surfaces with a scan size of 5 µm × 5 µm. The ion-implanted surface has a higher roughness of 0.67 nm as compared to the non-implant surface which is 0.17 nm, due to implantation-induced damage [10]. The SSRM profiles of the implanted and the non-implanted GaN are shown in Fig. 2(c). There is an increase in the resistivity of the implanted GaN, which can be attributed to either (i) the presence of damage-related defects or (ii) electrically active, and negatively charged fluorine ions formed during the implantation process which act as electron traps, thereby reducing the free carrier concentration and increases the resistance [11], or a combination of the two. To study the optical response of the implanted region, CL measurements were performed on the sample as shown in Fig.2(d). The CL measurement was obtained using a 5 keV electron beam at 4 K. In the non-implanted GaN, the CL spectra is dominated by a 358 nm peak, which corresponds to the near band edge (NBE) emission of GaN. Whereas, in the implanted region, this peak disappears completely. Such quenching on the NBE peak in implanted GaN has been reported previously for CL, and also for photoluminescence (PL) [12], [13]. To understand the impact of fluorine implanted GaN further, µ-Raman was used to examine the A_1(LO) peak position. As observed from Fig. 2(e), which is a false-color map of the peak position across an entire with mesa diameter to 340 µm, the implanted area can be distinguished due to a lower peak position. As this peak is sensitive to the free negative carrier concentration of the material [14], a lower value signifies a lower

doping. Fluorine implantation seems to have compensated the free carrier in the implanted region. The mean of A_1(LO) peak position in the non-implanted region was 733.3 cm^{-1} whereas for the implanted region, the mean position was lowered to 733.2 cm^{-1}.

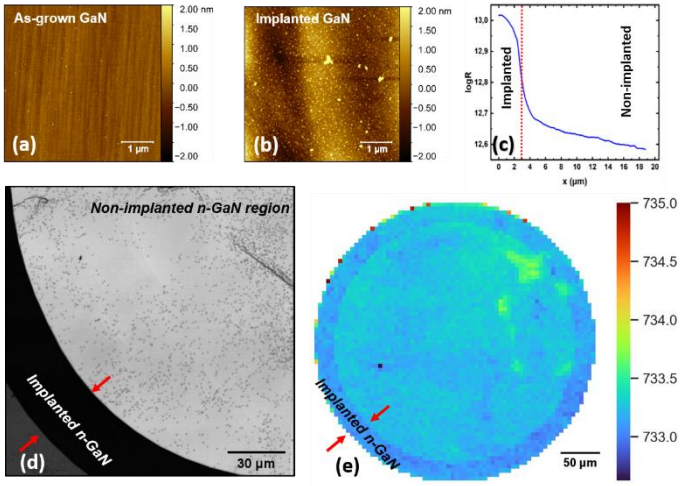

Figure 2. Implant induced change in surface morphology. (a) AFM image of non-implanted GaN surface . (b) AFM of implanted GaN surface (c) SSRM profile measured at implant/non-implant interface (d) Cathodoluminescence map of one corner of a diode. (e) µ-Raman A_1(LO) peak position map of a 340 µm diameter diode.

3.2. Electrical characterization

To investigate the influence of fluorine implant on the device parameters, six devices with a constant non-implant Schottky radius and incremental implant overlapped contact area were analysed and compared with a non-implanted control diode (Fig. 1-b). Two methods were used to extract the Schottky contact barrier height: (i) by extrapolating semi-log J vs V measurement to V = 0 and (ii) by taking the intercept on x-axis of $1/C^2$ vs V plot. The doping density as a function of depletion width was also extracted.

3.2.1. I-V characterisation

Fig. 3(a) shows the forward current density characteristics of the implanted, non-implant diode measured at RT, and the inset plot is the variation of ideality-factor (n) with respect to voltage extracted from equation (1).

$$n(V) = \frac{q}{kT} J_s \frac{\partial V}{\partial(\ln(J))} \qquad (1)$$

$$\emptyset_B^{I-V} = \frac{kT}{q} \ln\left(\frac{A^* T^2}{J_s}\right) \qquad (2)$$

where V is the applied bias, J the measured current density, J_s the saturation current density obtained by extrapolating semi-log J vs V curve to V = 0, A* the effective Richardson constant (taken at 26.4A/cm².K² for GaN for this study), k the Boltzmann constant, q the elementary charge, T the temperature and $\emptyset_B^{I-V}$ the barrier height extracted from I-V measurements.

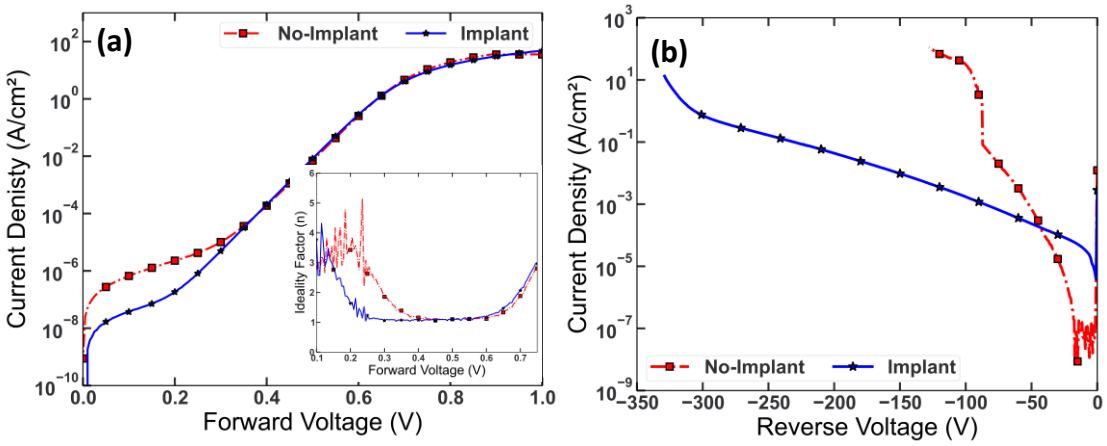

Figure 3. (a) Forward characteristic (b) Reverse characteristic of implant and non-implant didoe. The inset plot in (a) shows the variation in ideality factor as a function of forward voltage

The extracted ideality factor is equal to unity for both implanted and non-implanted diodes, suggesting thermionic emission over the potential barrier dominates the conduction mechanism. Barrier height $\emptyset_B^{I-V}$ determined by using Eq. (2) gives a value of 0.97 eV. The breakdown characteristics of the implanted and non-implanted diodes are presented in Fig. 3(b). Below -50 V, the reverse leakage current is lower in the non-implanted device compared to the implanted device but the leakage current slope is higher in the non-implanted device and undergoes a destructive breakdown at around -75 V whereas the implanted device performs better with a breakdown voltage (BV) of -365 V. However, this BV is still far from the parallel plane BV for the given drift layer doping and thickness and the cause is being investigated further. This is possibly related to defectivity of the substrate based on initial investigation.

3.2.2. C-V characterization

C-V measurements were performed at RT with a 1MHz frequency. These permit an analysis of the influence of implantation on the doping and barrier height in the different samples. The total capacitance as a function of applied reverse voltage is given by equation (3) and can be used to determine the net doping concentration ($N_d - N_a$), depletion width (W_D), and barrier height ($\emptyset_B^{C-V}$) using the following equations :

$$C_{total} = A\left[\frac{q\varepsilon_0\varepsilon_r N_D}{2\left(\varphi_{bi} - V - \frac{kT}{q}\right)}\right]^{\frac{1}{2}} = \frac{\varepsilon_0\varepsilon_r A}{W_D} \quad (3)$$

$$N_d - N_a = \frac{2}{q\varepsilon_0\varepsilon_r A^2\left(\frac{d(C^{-2})}{dV}\right)} \quad (4)$$

$$\emptyset_B^{C-V} = \varphi_{bi} + \emptyset_n + \frac{kT}{q} \quad (5)$$

$$\emptyset_n = \frac{kT}{q}\ln\left(\frac{N_C}{N_D}\right) \quad (6)$$

$\boldsymbol{\varepsilon_0}$ is the permittivity of free space (8.854×10^{-12} Fm^{-1}), $\boldsymbol{\varepsilon_r}$ the relative dielectric constant of GaN , A the total area of the Schottky contact, $\emptyset_n$ the position of Fermi level with respect to the conduction band, N_c the effective density of states in the conduction band and φ_{bi} the built-in potential in eV determined from the x-axis intercept of the A^2/C^2 vs V plot.

Fig. 4(a) shows the A/C^2 evolution as a function of the applied voltage enabling us to extract φ_{bi} values by linear fitting of the A/C^2 curves for the different structures. Using equation (5) and (6) the C-V barrier height ($\emptyset_B^{C-V}$) is calculated. It is observed that with an increase in implant overlap under the Schottky contact, φ_{bi} increases from 0.83 eV for the non-implanted device to 1.8 eV for the device with largest implant area (device 6, Fig. 1-b). The saturation current density extracted from the J-V method remained the same irrespective of the implant area as presented in Fig 4 (b) thus giving a constant barrier height ($\emptyset_B^{I-V}$). Fig. 4 (d) summarises the barrier height extracted from both the methodologies.

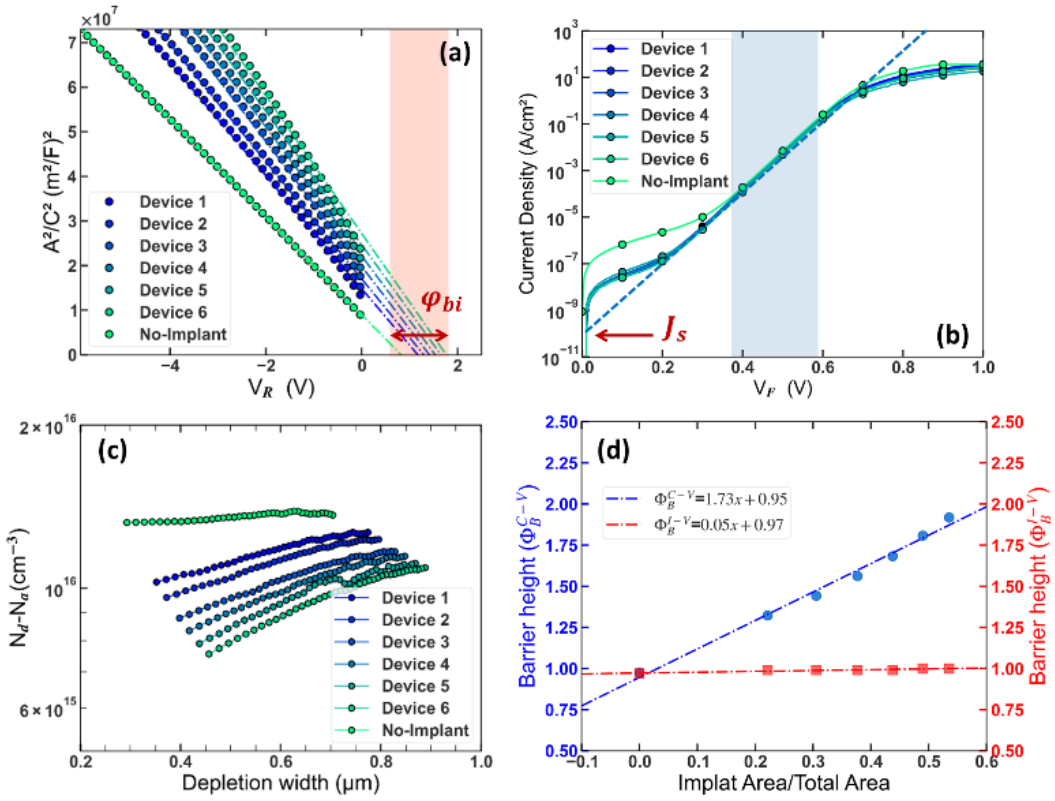

Figure 4. (a) Built in potential (φ_{bi}) extraction from A/C². (b) Saturation current density (J_s) extracted from linear fitting semi-log current density vs voltage plot. (c) Net doping concentration vs depletion width extracted for different devices (d) Barrier heights extracted from I-V (in red) and C-V (in blue) methods with respect to implant area divided by total contact area ratio.

These observations leads to two hypothesis:

a. Two independent barriers can be associated respectively with the implanted and non-implanted contact regions and the effective barrier is determined by the implant area under the Schottky contact in C-V measurements as:

$$\emptyset_B^{C-V} = 1.73\ x + 0.95\ eV$$

Where x is the ratio of implant area under the Schottky contact divided by the total contact area. From this equation, the barrier height of a fully implanted diode (x=1) is determined to be 2.73 eV.

b. The extracted barrier height extracted using I-V depends predominantly on the low barrier of non-implanted region.

$$\emptyset_B^{I-V} = 0.05\ x + 0.97\ eV$$

The net doping concentration as a function of depletion depth is plotted in Fig. 4(c). The doping concentration of the non-implanted diode remains almost constant at 1.3×10^{16} cm^{-3} throughout the depletion width. For the implanted device, the net-doping concentration reduces with increasing implant overlap under the Schottky contact. This confirms the reduction of free carrier concentration in the implanted region as observed through SSRM and μ-Raman mapping and can be explained by either the formation of negative fixed charge by fluorine or by a deep acceptor which captures free electrons and depletes the free carriers [15], [16]. This also explains the higher potential barrier as observed from the C-V measurements as negative fixed charges or deep electron traps may lead to the upward bending of the valence band and thus a higher barrier.

3.3. TCAD simulation

TCAD simulations, using commercially available Synopsys™ Sentaurus TCAD software, were performed to interpret the electrical results. A two-dimension structure as shown in Fig. 5(a) was generated and fixed negative charges were introduced at the contact edge to reproduce electrical modifications due to the fluorine implant. The negative charge profile was modeled using a SIMS profile (not shown here), which had a Gaussian like profile with a peak concentration of 2×10^{18} cm^{-3} at 43 nm depth. The thermionic emission model was used as the conduction mechanism to model current in the device as this was found to be the dominant conduction mechanism based on the ideality factor extracted from J-V measurements. Other recombination and tunneling models were therefore deactivated. The metal work function was adjusted to fit the experimental J-V curves and a good agreement between the experimental and TCAD simulated J-V was found for a TCAD barrier height of 0.97 eV, which is the experimentally extracted barrier height from J-V measurements. This validates that the models included in the simulation are accurate.

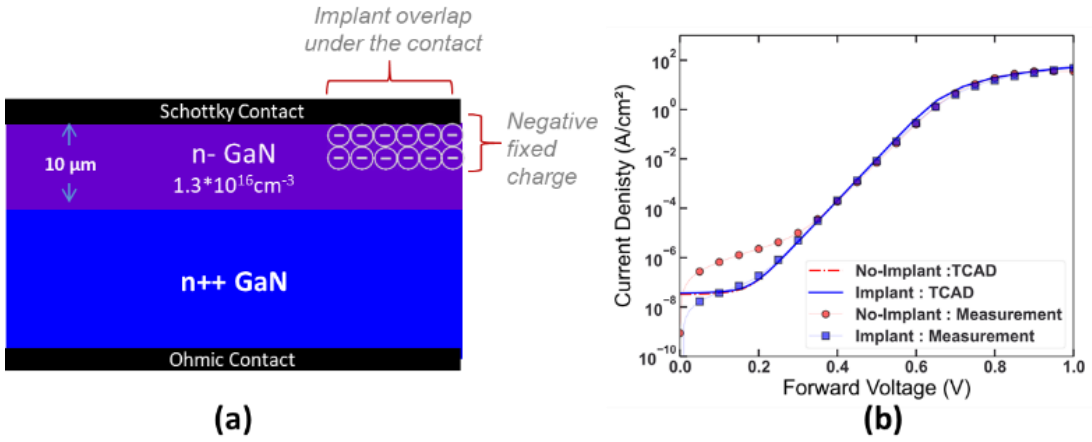

Figure 5. (a) 2D structure with fixed negative charge used in the simulation. (b) TCAD simulated and experimental J-V plot for both implant (blue) and non-implant (red) diode.

To investigate the influence of fixed negative charges on the band bending, the peak concertation of the negative charge was scaled. Fig. 6(a) represents the effective barrier height in the implanted region as a function of peak fixed charge concentration. Clearly, as the concentration of negative fixed charge increases, the valence band moves closer to the Fermi level due to the band bending in the space charge region near the GaN surface. This increases the effective barrier height by a value $\Delta\emptyset_F$ until the valence band is close enough to the Fermi level. From the C-V measurements, the implant area barrier height was estimated to be 2.73 eV, which corresponds to a peak negative charge concentration of 2×10^{17} cm^{-3}. This suggests that only around 10 % of the implanted fluorine exists as fixed negative charge. The band diagram at 0 V obtained from TCAD simulation is plotted in Fig. 6(b) for the non-implanted region (in red) and for the implanted region (in blue) for a fixed charge density of 2×10^{17} cm^{-3}.

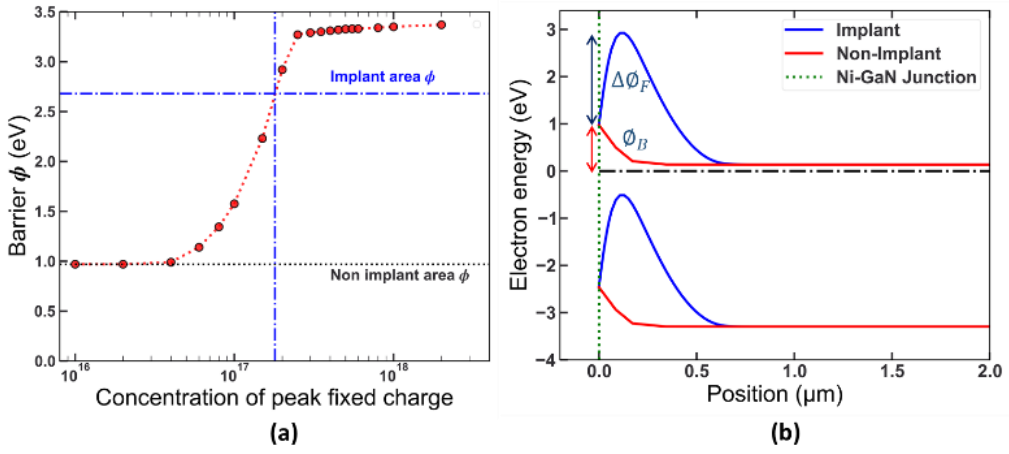

Figure 6. (a) Barrier height variation versus increasing peak concentration of fixed charge as obtained from TCAD simulations. (b) Bandgap of non-implant region (red) and implant region (blue) at 0 V.

4. Conclusion

In this study, vertical GaN-on-GaN Schottky structures were fabricated including planar edge terminations using multi-energy fluorine implantation and these were investigated by a series of characterizations. We found a reduction in free charge concentration in the implanted region extracted from the μ-Raman A1(LO) peak position which is sensitive to free carrier concentration, and a higher resistance by SSRM measurements. This is further confirmed by doping extracted from C-V measurements. Barrier height of the metal-GaN contact was extracted using I-V and C-V measurements. C-V measurements show an increase in the barrier height compared to the device without implantation, which increases linearly with the increase in the implant overlap under the Schottky contact. This suggests that effective barrier to be dependent on the area ratio while the barrier height extracted from I-V method remained constant. We postulate the existence of a double barrier connected in parallel: a low barrier associated with the non-implanted region of the Schottky contact and a high barrier associated with the implanted region due to the presence of fixed negative charges under the contact. The I-V measurements lead to the same barrier irrespective of the implant area as the lower barrier governs the forward current. However, in the C-V measurements, due to the formation of fixed negative charges in the implanted area, the space charge region width is modified leading to increasing intercept voltage with increasing area of implant under the contact and thus a higher barrier height. These observations from I-V and C-V measurements were successfully modelled by TCAD simulations using Synopsys® SentaurusTM by including negative fixed charge under the contact edge using fluorine profile obtained by SIMS. Using the simulation and the barrier height extracted from C-V measurements for the implanted region, we were able to estimate that only a small percentage (10 % in our case) of implanted fluorine exists as negative charges. This is an important parameter to be considered while designing efficient edge terminations using fluorine implantation as the energy and fluence of the implantation will need to be adjusted to take into account this difference.

5. Acknowledgment

This work is part of the VertiGaN project supported by the labex GANEXT.

6. References

[1] C. Le Royer *et al.*, “Normally-OFF 650V GaN-on-Si MOSc-HEMT Transistor: Benefits of the Fully Recessed Gate Architecture,” *Proc. Int. Symp. Power Semicond. Devices ICs*, vol. 2022-May, pp. 49–52, 2022, doi: 10.1109/ISPSD49238.2022.9813672.

[2] D. Khachariya *et al.*, "Vertical GaN junction barrier Schottky diodes with near-ideal performance using Mg implantation activated by ultra-high-pressure annealing," *Appl. Phys. Express*, vol. 15, no. 10, 2022, doi: 10.35848/1882-0786/ac8f81.

[3] C. W. Chen, L. Y. Kuo, Y. C. Lai, and Y. ming Hsin, "Vertical GaN Schottky Barrier Diode Using Nitrogen Ion Implantation to Form a Donut-Shaped Channel," *J. Electron. Mater.*, vol. 50, no. 9, pp. 5453–5461, 2021, doi: 10.1007/s11664-021-09080-7.

[4] A. M. Ozbek and B. J. Baliga, "Finite-zone argon implant edge termination for high-voltage gan schottky rectifiers," *IEEE Electron Device Lett.*, vol. 32, no. 10, pp. 1361–1363, 2011, doi: 10.1109/LED.2011.2162221.

[5] S. Koné, F. Cayrel, A. Yvon, E. Collard, and D. Alquier, "DLTS analysis of high resistive edge termination technique-induced defects in GaN-based Schottky barrier diodes," *Phys. Status Solidi Appl. Mater. Sci.*, vol. 213, no. 9, pp. 2364–2370, 2016, doi: 10.1002/pssa.201532895.

[6] W. Khalfaoui *et al.*, "Impact of rapid thermal annealing on Mg-implanted GaN with a SiOx/AlN cap-layer," *Physica Status Solidi (A) Applications and Materials Science*, vol. 214, no. 4. 2017, doi: 10.1002/pssa.201600438.

[7] K. J. Chen, "Fluorine plasma ion implantation technology: A new dimension in GaN device processing," *Int. Conf. Solid-State Integr. Circuits Technol. Proceedings, ICSICT*, pp. 1074–1077, 2008, doi: 10.1109/ICSICT.2008.4734737.

[8] R. Yin *et al.*, "High Voltage Vertical GaN-on-GaN Schottky Barrier Diode with High Energy Fluorine Ion Implantation Based on Space Charge Induced Field Modulation (SCIFM) Effect," *Proc. Int. Symp. Power Semicond. Devices ICs*, vol. 2020-September, pp. 298–301, 2020, doi: 10.1109/ISPSD46842.2020.9170190.

[9] S. Han, S. Yang, and K. Sheng, "Fluorine-implanted termination for vertical GaN schottky rectifier with high blocking voltage and low forward voltage drop," *IEEE Electron Device Lett.*, vol. 40, no. 7, pp. 1040–1043, 2019, doi: 10.1109/LED.2019.2915578.

[10] S. O. Kucheyev, J. S. Williams, J. Zou, C. Jagadish, and G. Li, "High-dose ion implantation into GaN," in *Nuclear Instruments and Methods in Physics Research, Section B: Beam Interactions with Materials and*

Atoms, Apr. 2001, vol. 175–177, pp. 214–218, doi: 10.1016/S0168-583X(00)00672-8.

[11] M. Usman, A. Nazir, T. Aggerstam, M. K. Linnarsson, and A. Hallén, "Electrical and structural characterization of ion implanted GaN," *Nucl. Instruments Methods Phys. Res. Sect. B Beam Interact. with Mater. Atoms*, vol. 267, no. 8–9, pp. 1561–1563, 2009, doi: 10.1016/j.nimb.2009.01.091.

[12] C. Uzan-Saguy *et al.*, "Electrical isolation of GaN by ion implantation damage: Experiment and model," *Appl. Phys. Lett.*, vol. 74, no. 17, pp. 2441–2443, 1999, doi: 10.1063/1.123874.

[13] S. O. Kucheyev, M. Toth, M. R. Phillips, J. S. Williams, C. Jagadish, and G. Li, "Cathodoluminescence depth profiling of ion-implanted GaN," *Appl. Phys. Lett.*, vol. 78, no. 1, pp. 34–36, 2001, doi: 10.1063/1.1337646.

[14] A. J. Eric N'Dohi *et al.*, "Micro-Raman characterization of homo-epitaxial n doped GaN layers for vertical device applications," *AIP Adv.*, vol. 12, no. 2, 2022, doi: 10.1063/5.0082860.

[15] M. J. Wang, L. Yuan, C. C. Cheng, C. D. Beling, and K. J. Chen, "Defect formation and annealing behaviors of fluorine-implanted GaN layers revealed by positron annihilation spectroscopy," *Appl. Phys. Lett.*, vol. 94, no. 6, pp. 1–4, 2009, doi: 10.1063/1.3081019.

[16] J. Xu *et al.*, "Experimental and theoretical study on device-processing-incorporated fluorine in AlGaN/GaN heterostructures," *AIP Adv.*, vol. 10, no. 6, 2020, doi: 10.1063/5.0005091.